Journal of Materials Science & Technology 198 (2024) 73–82

Contents lists available at ScienceDirect

Journal of Materials Science & Technology

journal homepage: www.elsevier.com/locate/jmst

Research Article

A 2D biobased P/N-containing aggregate for boosting fire retardancy of PA6/aluminum diethylphosphinate *via* synergy

Yixia Lu[a,b], Jiabing Feng[a,b,*], Tao Chu[a], Siqi Huo[a], Hongyan Xie[b], Zhiguang Xu[b,*], Hao Wang[a], Pingan Song[a,c,*]

[a] Centre for Future Materials, University of Southern Queensland, Springfield 4300, Australia
[b] China-Australia Institute for Advanced Materials and Manufacturing, Jiaxing University, Jiaxing 314001, China
[c] School of Agriculture and Environmental Science, University of Southern Queensland, Springfield, QLD 4300, Australia

ARTICLE INFO

Article history:
Received 28 January 2024
Revised 1 March 2024
Accepted 2 March 2024
Available online 12 March 2024

Keywords:
Melamine phytate aggregate
Fire-retardant PA6
Synergism
Aqueous reaction

ABSTRACT

Engineering polyamide 6 (PA6) is preferred for its superior mechanical properties, yet the intrinsic flammability restricts its industrial applications. As one of the biomass phosphorus-containing chemicals, phytic acid (PA) is favorable for its high phosphorus content and aggregation ability, making it expected to enhance the fire retardancy of PA6. Herein, a melamine-phytate aggregate (MPA) is prepared by electrostatic interaction in aqueous solution, and applied as a synergist for aluminum diethylphosphinate (ADP) in PA6. The strong synergistic effect exists between ADP and MPA towards PA6, especially when their mass ratio is 3:1 and the total loading is 18 wt%. Compared to the neat PA6, this formula allows for remarkable decreases in peak heat release rate (PHRR), total heat release (THR), and maximum average heat release rate (MARHE) by ~ 48 %, ~ 27 %, and ~ 30 %, respectively, as well as a high synergistic efficiency of ~ 43 % in PHRR. This PA6 composite also presents a V-0 rating in the vertical burning (UL-94) test and a high limiting oxygen index (LOI) of 29.7 %. This work offers an eco-friendly strategy for developing bio-based P/N fire-retardant aggregates for fabricating PA6 materials with high fire safety.

1. Introduction

Owing to the superior performances including mechanical strength, oil resistance, self-lubrication, and attrition resistance, polyamide 6 (PA6) has been ubiquitously used as a significant engineering material in various areas, such as electrical and electronic fields, manufacturing, and packaging [1–3]. However, PA6 can easily cause fire due to its intrinsic flammability, high heat release, melt-dropping, and toxic gases, thus leading to casualties and property loss. Such fire risks significantly restrict its practical applications where high fire safety is required, e.g., electrical appliances [4–6]. Thus, it is imperative to develop fire-retardant PA6 materials.

As a prominent category of halogen-free fire retardants, phosphorus-based fire retardants (P-FRs) offer a favorable solution to mitigate fire hazards of polymeric materials. During combustion, they can act both in the condensed and gas phases, by producing phosphorus/phosphate salts to facilitate the char formation and generating PO• radicals to scavenge high-energy HO• and H• radicals, thus suppressing the burning reaction [7–14]. Over the last decade, biomass materials have gained great attention due to their environmental-friendly features [15–18]. Phytic acid (PA), with a high P content (28 wt%) and an inositol hexaphosphate structure, has been extensively explored in the preparation of fire-retardant polymers because of its renewable feature (from beans, cereal grains, seeds, etc.) and low cost [19–23]. Apart from promoting char-formation and trapping active radicals, it can also enhance the anti-melting performance of polymeric matrices via dehydration reactions to form P–O–P structures [17,24,25]. Nevertheless, PA is not usually applied alone because of its strong acidity and migration, which might reduce the mechanical performances of matrices, in addition to the easy thermal degradation [5].

To address these issues, the metal-chelating PA-Zn [26], PA-Ni [27], and PA-Mg [28] have been developed and applied in different polymer matrixes. Besides, amines are considered as good candidates to ameliorate the acidity of PA as their amino groups can easily react with $-P(O)(OH)_3$ groups of PA [29–31]. Meanwhile, the fire retardancy of polymers could be highly improved by phosphorus/nitrogen (P/N)-based fire retardants owing to their synergistic fire-retardant effects [2,32–36]. For example, polypropylene (PP)

* Corresponding authors at: Centre for Future Materials, University of Southern Queensland, Springfield 4300, Australia.
E-mail addresses: jiabing.feng@zjxu.edu.cn (J. Feng), zhiguang.xu@zjxu.edu.cn (Z. Xu), pingan.song@usq.edu.au, pingansong@gmail.com (P. Song).

https://doi.org/10.1016/j.jmst.2024.03.001

with 18 wt% of phytic acid salt (PHYPI) showed an increased LOI of 25.0 %, an UL-94 V-0 rating, and enhanced char-forming ability [37]. In addition, triethanolamine (TEA) was applied as a blowing agent to adjust the acidity and enhance the fire retardancy of PA-loaded cotton fabrics [38]. Furfurylamine phytate (PAF) was prepared in ethanol solution and 2 phr of it endowed poly (lactic acid) (PLA) with a high LOI value of 34.2 % [39]. Recently, a phytic acid/silane hybrid sol was synthesized by using PA and silane (3-(2aminoethylamino)-propyltrimethoxysilane (AAPTMS) as raw materials, which significantly increased the LOI of cotton fabrics to 31.0 % [19]. Although the superior charring ability of PA is highly desired in preparing fire-retardant PA6, PA-derived fire retardants for PA6 are rarely reported.

Melamine (MA) and its derivatives are regarded as favorable nitrogen sources that produce inert gases (e.g., NH_3) to dilute oxygen during combustion, and thus they have been used in fire-retardant PA6 widely [8,40]. Therefore, it is expected to enhance the fire safety of PA6 by developing an MA-PA flame retardant based on the reaction between $-NH_2$ and $-P(O)(OH)_3$. On the other hand, in case of the unstable char layers caused by the release of excessive inert gases from amino-rich MA, the commercial aluminum diethylphosphinate (ADP) is expected to maintain partial N atoms in the condensed phase and then manipulate the char formation, to finally enhance the quality of char layers and fire retardancy of PA6 [41–43].

This work targets at developing a plant-derived P/N-containing fire-retardant synergist via a green reaction for the PA6/ADP system. PA and melamine are chosen to assemble a supramolecular aggregate (MPA) via electrostatic interaction in water. The as-synthesized MPA shows a strong synergism with ADP when used in PA6. Specifically, the combination of 4.5 wt% MPA and 13.5 wt% ADP imparts high fire safety to PA6, with an LOI of ~30 %, a UL-94 V-0 rating, and a low peak heat release rate (PHRR) (reduced by ~48 % compared to that of pure PA6). This study provides a green approach for preparing bio-based flame-retardant system for high-performance PA6 that is urgently needed in end-use industries.

2. Experimental section

2.1. Materials and reagents

PA6 (Durethan BC30) was provided by Lanxess Energizing Chemistry Co. (Germany). Melamine (MA), phytic acid aqueous solution (70 %), and aluminum diethylphosphinate (ADP) were purchased from Macklin Inc. (China). All chemicals were used directly without prior treatment. Ultrapure water (18.2 MΩ) was produced by a Merck Millipore Ultrapurification system.

2.2. Synthesis of MPA

Three different molar ratios of MA/PA (6:1, 4:1, 3:1) were used to explore the effect of the molar ratio of the starting materials on the structure of the final MPA products. X-ray photoelectron spectroscopy (XPS) results (Table S1 in the Supplementary Material) and SEM images (Fig. S1) indicate that there is no distinct difference in elemental composition and micromorphology of MPA. To ensure the complete reaction, a reaction molar ratio of 6:1 (MA/PA) was used. Firstly, 18.9 g of MA was stirred continuously with 600 mL of ultrapure water in a flask at 90 °C, whilst 23.6 g of phytic acid aqueous solution (70 %) was diluted to 60 mL. Then, the obtained phytic acid solution was added dropwise into the MA aqueous solution using a pressure-equalizing dropping funnel. The light greyish solid powder was generated progressively, and the mixture was stirred for 2 h. Lastly, the powder (MPA) was obtained by filtration, washing with hot water 3 times, and vacuum drying at 100 °C overnight.

2.3. Preparation of fire retardant PA6/MPA/ADP (FRPA6) composite

PA6 pellet was dried at 80 °C for 4 h before use, and then it was melt-blended with MPA and ADP at 220 °C for 6 min with a rotor speed of 60 r/min in a torque rheometer (RM-200C, HAPRO), followed by hot-pressing into desirable testing specimens at 230 °C under 10 MPa for 2 min and cool-pressing. The as-prepared FRPA6 composites containing various proportions of MPA and ADP with a total addition of 18 wt% were named as PA6/MPA_{18}, PA6/MPA_6/ADP_{12}, PA6/MPA_5/ADP_{13}, PA6/$MPA_{4.5}$/$ADP_{13.5}$, PA6/$MPA_{3.6}$/$ADP_{14.4}$, PA6/MPA_3/ADP_{15}, and PA6/ADP_{18}, respectively, where the number represented the addition amount. PA6 specimens were fabricated in the same process without the addition of fire retardants.

2.4. Characterizations and measurements

Fourier transform infrared (FT-IR) spectra were obtained by an FTIR spectrometer (Thermofisher IS50). X-ray diffraction (XRD) was conducted on an X-ray diffractometer (XRD-7000, Shimadzu) with Cu Kα radiation ($\lambda = 0.1542$ nm). XPS was performed on a Thermo Scientific K-Alpha with Al Kα radiation ($h\nu = 1486.6$ eV). Thermogravimetric analysis (TGA) was undertaken on a thermogravimetric analyzer (DSC3+/TRACE 1300-ISQ7000, Thermo Fisher Scientific) from 25 to 800 °C with a heating rate of 10°C/min under nitrogen or air atmosphere. Scanning electron microscope (SEM) and energy dispersive spectroscopy (EDS) were carried out on a Helios 5CX (Thermo Fisher Scientific). Transmission electron microscope (TEM) was conducted on a Talos F200X (Thermo Fisher Scientific).

Vertical burning (UL-94) test was performed on a Jiangning CZF-2 instrument, with a sample dimension of 130 mm × 13 mm × 3.2 mm. Limiting oxygen index (LOI) was obtained by using a JF-3 type oxygen index meter, and the sample dimension was 80 mm × 10 mm × 4 mm in accordance with ASTM D2863-2009. Cone calorimetry test was performed on a calorimeter (FTT, UK) with a heat flux of 50 kW/m^2 according to ISO 5660, with a specimen size of 100 mm × 100 mm × 3.0 mm. Thermogravimetric-infrared spectrometry (TG-IR) was carried out on a thermogravimetric analyzer (TGA8000, PerkinElmer) and FT-IR spectrometer (Spectrum 3, PerkinElmer). Mechanical properties were investigated by an electronic universal testing machine (UTM2503, Sans) with a cross-head rate of 5.0 mm/min. All samples were prepared based on GB/T 1040.

To assess the fire safety of FRPA6, fire performance index (FPI) and fire growth index (FGI) are calculated by the following Eqs. (1) and (2).

$$\mathrm{FPI} = \mathrm{TTI}/\mathrm{PHRR} \tag{1}$$

$$\mathrm{FGI} = \mathrm{PHRR}/\mathrm{Time\ to\ reach\ PHRR} \tag{2}$$

where TTI is abbreviated for time to ignition.

To explore the synergistic effect (SE) between MPA and ADP with various ratios in FRPA6 composites, here the SE values referring to PHRR, total heat release (THR), and effective heat of combustion (EHC) are calculated based on Eqs. (3) and (4) [44]:

$$P_{\mathrm{Calculated}} = P_{\mathrm{MPA}} \times \phi_{\mathrm{MPA}} + P_{\mathrm{ADP}} \times \phi_{\mathrm{ADP}} \tag{3}$$

$$\mathrm{SE} = \left(P_{\mathrm{Calculated}} - P_{\mathrm{Experimental}}\right)/P_{\mathrm{Calculated}} \tag{4}$$

where P is the parameter obtained from the cone calorimeter test, referring to PHRR, THR, and EHC. ϕ is the ratio of MPA or ADP in FRPA6 containing 18 wt% of MPA and ADP.

To explore the fire-retardant mechanism of FRPA6, the flame inhibition, charring effect, and barrier-protective effect are calculated

by Eqs. (5)–(7) based on the data obtained from cone calorimetry tests:

$$\text{Flame inhibition} = 1 - \text{EHC}_{\text{FRPA6}}/\text{EHC}_{\text{PA6}} \quad (5)$$

$$\text{Charring effect} = 1 - \text{TML}_{\text{FRPA6}}/\text{TML}_{\text{PA6}} \quad (6)$$

$$\text{Barrier} - \text{protective effect} = 1 - (\text{PHRR}_{\text{FRPA6}}/\text{PHRR}_{\text{PA6}})/(\text{THR}_{\text{FRPA6}}/\text{THR}_{\text{PA6}}) \quad (7)$$

where TML represents total mass loss during the cone calorimetry test.

3. Results and discussion

3.1. Characterization of MPA

Fig. 1(a) illustrates the synthesis route of MPA. The aggregate MPA is formed *via* the electrostatic interaction between $-NH_2$ of MA and $-P(O)OH$ of PA in aqueous solution. The FTIR spectra of MA, PA, and MPA are depicted in Fig. 1(b). For MA, the absorption peaks at 3470, 3417, 3334, and 3127 cm^{-1} are attributed to the stretch vibration of the $-NH_2$ group, while the peaks at 1652, 1553, and 1026 cm^{-1} belong to the N–H bending, C=N, and C–N vibrations, respectively [44]. The FTIR spectrum of PA demonstrates the absorption of P=O and P–O at 1364 and 778 cm^{-1}, respectively. Upon the formation of MPA, the absorption peaks of the $-NH_2$ group shift to 3360 and 3147 cm^{-1}, and those of N–H, C=N, and C–N slightly shift to 1675, 1510, and 1060 cm^{-1}, respectively, owing to the electrostatic interaction of MA and PA. Additionally, the absorption peaks of P=O and P–O appear at 1180 and 778 cm^{-1}, respectively. More importantly, the distinct peak at 1675 cm^{-1} indicates the formation of $-NH_3^+$. These results verify the successful synthesis of MPA.

Fig. 1(c) shows the elemental constitution of MPA by XPS, including carbon (C_{1s}, 288.2 eV), nitrogen (N_{1s}, 399.0 eV), oxygen (O_{1s}, 531.7eV), and phosphorus (P_{2p}, 133.1 eV). In the high-resolution N_{1s} spectrum (Fig. 1(d)), the binding energy peaks at 399.1 and 398.4 eV are ascribed to C–N and C=N bonds of the triazine ring from MA, and that at 400.8 eV is attributed to the $-NH_2$ group, indicating that partial $-NH_2$ groups are unreacted in

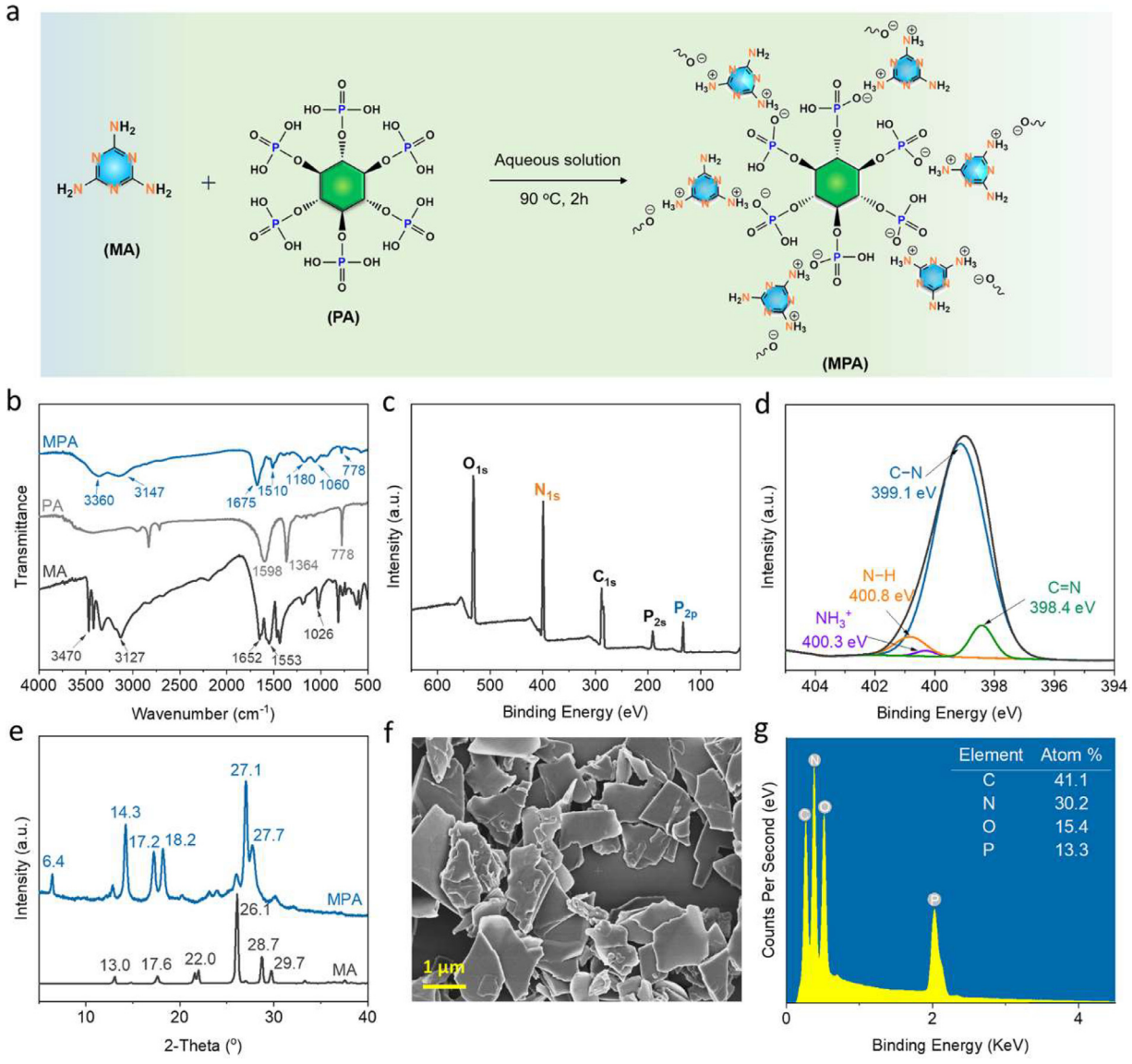

Fig. 1. Synthesis and characterization of MPA: (a) synthesis route of MPA, (b) FTIR spectra of MPA, PA, and MA, (c) XPS full-scan spectrum of MPA, (d) high-resolution XPS N_{1s} spectrum of MPA, (e) XRD patterns of MPA and MA, (f) SEM image of MPA, and (g) EDS graph of MPA.

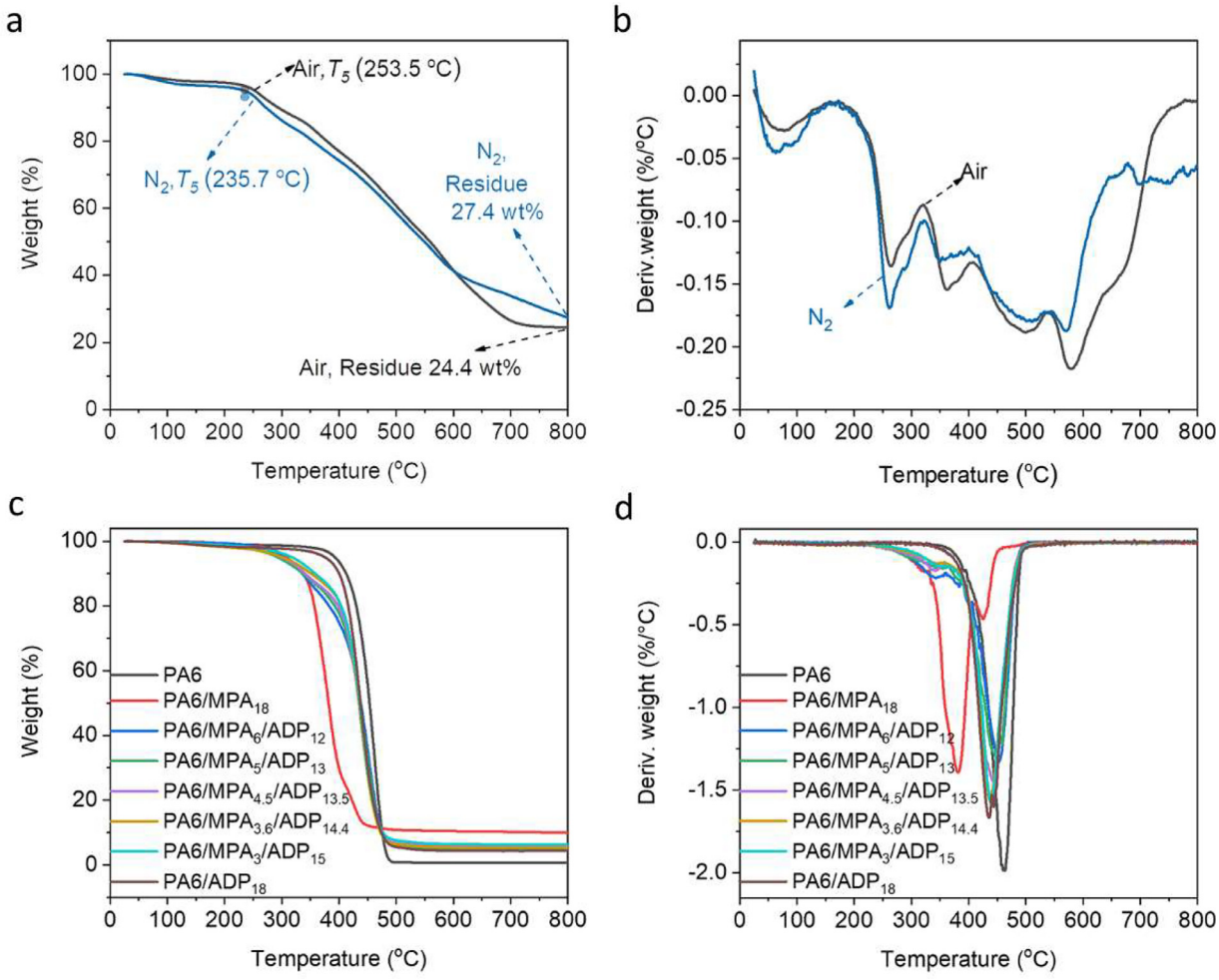

Fig. 2. (a) TGA and (b) DTG curves of MPA under air/N_2 atmosphere; and (c) TGA and (d) DTG curves of PA6 and FRPA6 composites in N_2 condition.

MPA. Additionally, the peak at 400.3 eV reveals the existence of the $-NH_3^+$ group. The XPS results are in line with the FTIR ones, demonstrating the formation of MPA.

XRD is another technique to explore the material structure. As shown in Fig. 1(e), the peaks at 13.0°, 17.6°, 22.0°, 26.1°, 28.7°, and 29.7° belong to (−101), (−111), (210), (−301), (−311), and (310) planes of MA, which is in consistent with the standard JCPDS card No. 24-1654 [45]. Upon the reaction with PA, new peaks appear at 6.4°, 14.3°, 17.2°, 18.2°, 27.1°, and 27.7° in the XRD pattern of MPA, which reveal the crystal structure difference between MPA and MA. Additionally, MPA exhibits a typical two-dimensional supramolecular aggregated structure, as reflected by the micro-scale flakes with sizes of 0.5–3 μm and thicknesses of 30-60 nm in Fig. 1(f). As shown in EDS spectrum (Fig. 1(g)), MPA contains 41.1 % of C, 15.4 % of O, 30.2 % of N, and 13.3 % of P. In brief, all these results demonstrate the successful synthesis of MPA *via* a facile and green approach.

3.2. Thermal decomposition behaviors

TGA and derivative TGA (DTG) results (see Fig. 2 and Table 1) illustrate the thermal stability of MPA under air and nitrogen atmosphere, respectively. The temperature at 5 % mass loss (T_5) of MPA is 236 °C (N_2)/254°C (air), which is above the melt-blending temperature of PA6 composite (220–230 °C), indicating it keeps stable during melt-blending. In addition, the temperature at maximum weight loss rate (T_{max}) of MPA is 570 °C (N_2)/580°C (air), and its maximum mass loss rate (R_{ml}) is 0.19 wt%/°C (N_2)/0.22 wt%/°C (air). Notably, the char yield of MPA at 800°C reaches up to 27.4 wt% (N_2)/24.4 wt% (air), demonstrating its desirable charring ability. In summary, MPA exhibits high thermal stability in both nitrogen and air conditions, and its excellent charring ability is highly needed in the preparation of fire-retardant PA6.

Pure PA6 shows satisfactory thermal stability with a T_5 of 393.2 °C and a T_{max} of 461.8 °C, but poor charring ability, as confirmed by a char yield of only 0.7 wt%. With the incorporation of MPA, as expected, the char yield of the resulting PA6/MPA$_{18}$ increases to 9.9 wt%, but the T_5 and T_{max} decrease to 308.7 and 381.4 °C, which is due to the lower decomposition temperature of MPA itself. For commercial ADP, although its sole addition cannot bring a high char residue for PA6 as MPA does, it largely maintains the thermal stability of the PA6 matrix. For instance, PA6/ADP$_{18}$ shows a T_5 of 376.2 °C and a T_{max} of 436.0 °C. Clearly, the combination of MPA and ADP (18 wt%, totally) is expected to make the FRPA6 composites achieving moderate thermal stability and char-forming ability. For example, PA6/MPA$_{4.5}$/ADP$_{13.5}$ shows a char yield of 5.7 wt% with a T_{max} of 442.1 °C. As the ADP/MPA addition proportion increases to 5, the PA6/MPA$_3$/ADP$_{15}$ shows balanced thermal stability, as evidenced by its high T_5 (318.7 °C) and char residue (6.3 wt%), and a slightly reduced T_{max} (438.6 °C). It is also noted that MPA is helpful in alleviating the thermal degradation of the PA6 matrix at elevated temperatures. For instance, the R_{ml} value is 1.6 wt%/°C for PA6/MPA$_3$/ADP$_{15}$ (close to that of PA6/ADP$_{18}$), but it reduces to 1.2 wt%/°C for PA6/MPA$_6$/ADP$_{12}$. Such trend proba-

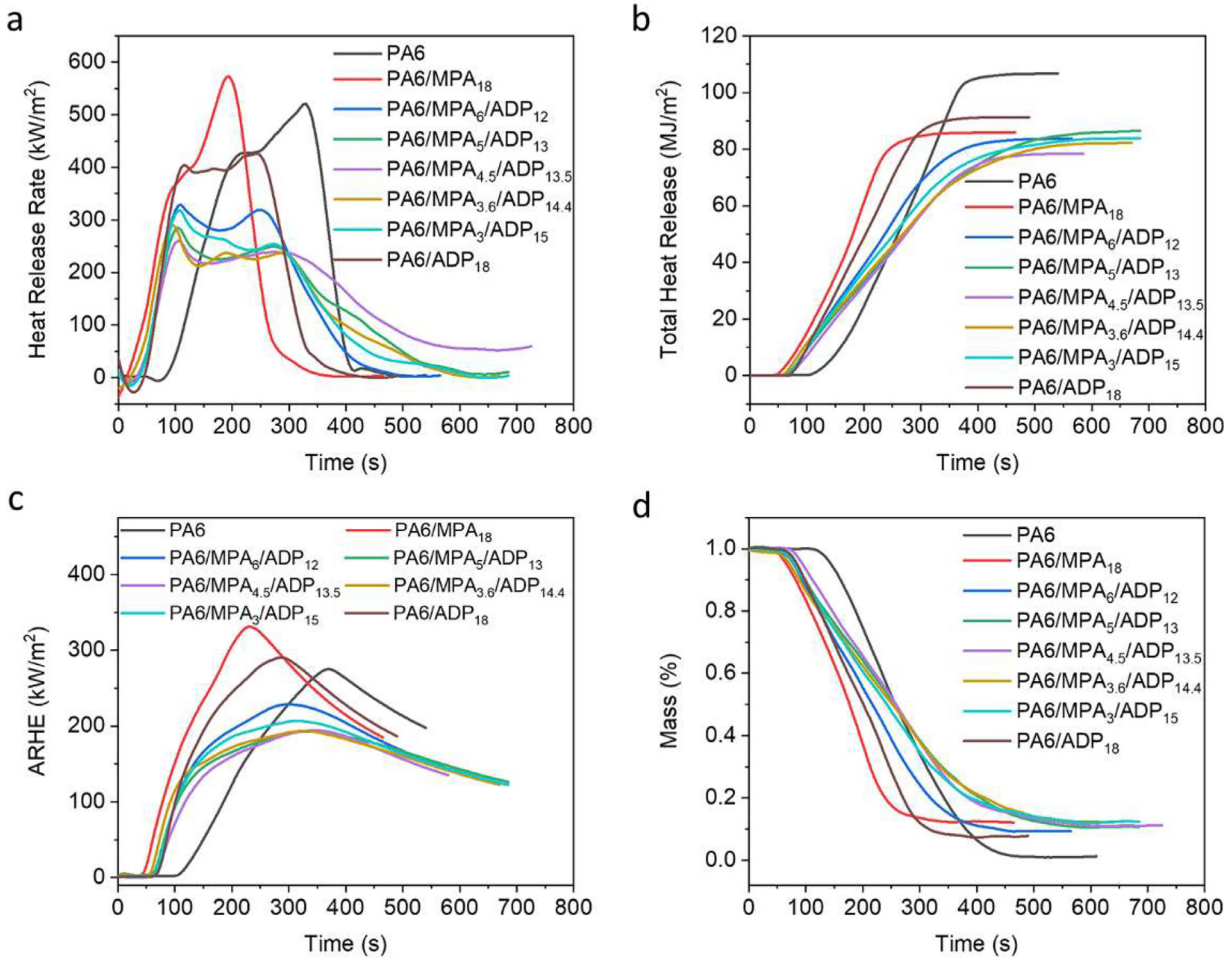

Fig. 3. Flammability performances of PA6 and FRPA6 evaluated by cone calorimeter tests: (a) HRR curves, (b) THR curves, (c) ARHE curves, and (d) mass loss curves.

Table 1
TGA results of MPA, PA6 and FRPA6 under nitrogen atmosphere.

Sample	[a]T_5 (°C)	[a]T_{max} (°C)	[b]R_{ml} (wt%/°C)	Residue at 800 °C (wt%)
MPA	235.7 (N_2) /253.5 (Air)	570.0 (N_2) /579.3 (Air)	0.19 (N_2) /0.22 (Air)	27.4 (N_2) /24.4 (Air)
PA6	393.2	461.8	2.0	0.7
PA6/MPA_{18}	308.7	381.4	1.4	9.9
PA6/MPA_6/ADP_{12}	304.9	452.1	1.3	5.9
PA6/MPA_5/ADP_{13}	293.7	447.0	1.3	4.8
PA6/$MPA_{4.5}$/$ADP_{13.5}$	299.7	442.1	1.4	5.7
PA6/$MPA_{3.6}$/$ADP_{14.4}$	302.5	437.7	1.6	5.3
PA6/MPA_3/ADP_{15}	318.7	438.6	1.6	6.3
PA6/ADP_{18}	376.2	436.0	1.7	4.3

[a] T_5 and T_{max} refer to the temperature at 5 % mass loss and the maximum mass loss rate, respectively.
[b] R_{ml} refers to the maximum mass loss rate.

bly results from the good charring ability of MPA. Consequently, the introduction of MPA into FRPA6 is expected to enhance high-temperature stability and suppress heat release during combustion [46].

3.3. Fire retardancy and synergistic mechanism

UL-94 and LOI tests were carried out to evaluate the fire safety of FRPA6 composites. As presented in Table 2, pristine PA6 is highly flammable with an UL-94 V-2 rating and a LOI value of 23.2 %. The addition of 18 wt% MPA fails to suppress the intrinsic flammability of PA6, and even slightly reduces its LOI, although MPA can promote the char-formation of PA6. On the contrary, the addition of ADP (18 wt%) enables PA6 to pass V-0 rating in the UL-94 test and obtains a high LOI of 34.1 %. With the combination of MPA and ADP, the resulting FRPA6 composites still present satisfactory fire retardancy. For instance, when 5 wt % MPA and 13 wt% ADP are introduced, the PA6/MPA_5/ADP_{13} sample exhibits a LOI of 26.8 % and a UL-94 V-0 rating. Then, as the ADP proportion increases to 15 wt%, the burning time of PA6/MPA_3/ADP_{15} during the UL-94 test further shortens to 3/0 s and the LOI value rises to 30.5 %.

The cone calorimetry test was conducted to further investigate the fire behaviors of PA6 and FRPA6. As demonstrated in Table 3 and Fig. 3(a, b), pure PA6 exhibits high flammability, as

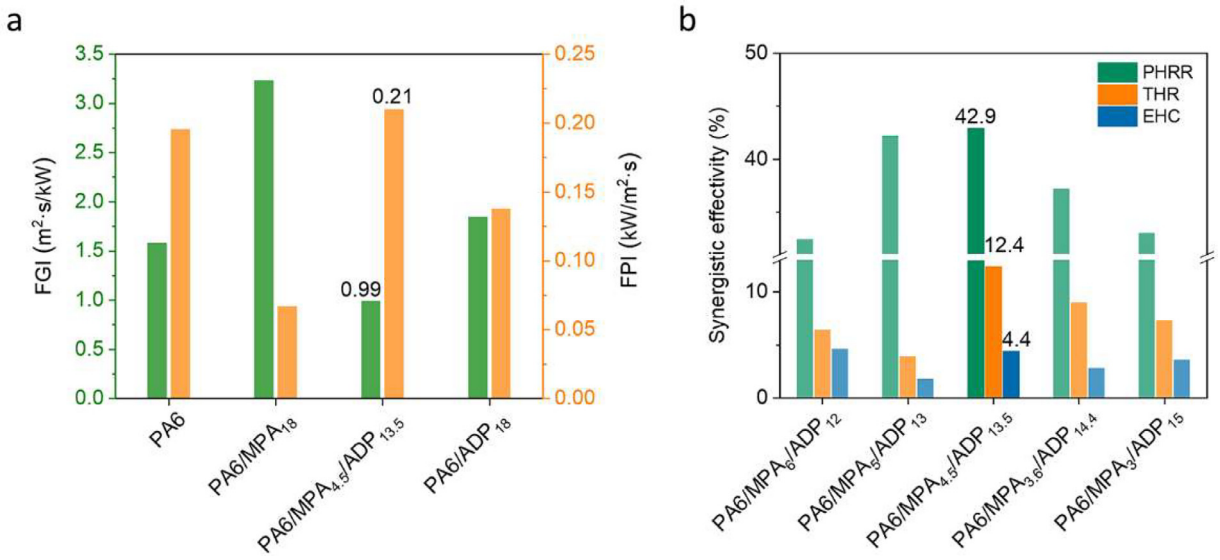

Fig. 4. (a) FGI & FPI values of PA6 and the typical three FRPA6; and (b) synergistic efficiencies of the five MPA/ADP-doped FRPA6 in PHRR, THR, and EHC.

Table 2
UL-94 ratings and LOI values of PA6 and FRPA6.

Sample	UL-94			
	t_1/t_2 [a](s)	Dripping/Cotton ignition	Rating	LOI (%)
PA6	19/7	Yes/Yes	V-2	23.2
PA6/MPA_{18}	17/37	Yes/Yes	V-2	21.5
PA6/MPA_6/ADP_{12}	15/4	No/No	V-1	23.5
PA6/MPA_5/ADP_{13}	9/6	No/No	V-0	26.8
PA6/$MPA_{4.5}$/$ADP_{13.5}$	8/5	No/No	V-0	29.7
PA6/$MPA_{3.6}$/$ADP_{14.4}$	6/3	No/No	V-0	30.4
PA6/MPA_3/ADP_{15}	3/0	No/No	V-0	30.5
PA6/ADP_{18}	3/0	No/No	V-0	34.1

[a] t_1 and t_2 refer to the burning time after the first and second ignition, respectively.

reflected by a high PHRR of 522.1 kW/m^2 and THR of 106.5 MJ/m^2, which are the two key parameters to evaluate the fire risk of polymer materials [47]. For PA6/MPA_{18}, it shows a higher PHRR (597.7 kW/m^2), implying a negative effect of MPA on the suppression of heat release. Such results are also in line with the lower LOI (21.5 %). On the other hand, in addition to reducing the THR to 91.2 MJ/m^2, the addition of 18 wt% of commercial ADP successfully decreases the PHRR to 442.6 kW/m^2. Upon combining MPA with ADP, excitingly, the FRPA6 composites present even lower combustion intensity than that of the PA6/ADP_{18} sample, which is mainly due to the synergism of MPA and ADP. For example, when the weight ratio of ADP/MPA reaches 2.6, the PHRR and THR values of PA6/MPA_5/ADP_{13} drop to 280.9 kW/m^2 and 86.3 MJ/m^2, respectively. As the ADP/MPA ratio is up to 3, the PHRR and THR values of PA6/$MPA_{4.5}$/$ADP_{13.5}$ further decrease to 272.9 kW/m^2 and 78.3 MJ/m^2 by 47.8 % and 26.5 % relative to those of PA6. Moreover, the maximum average rate of heat emission (MARHE) of PA6/$MPA_{4.5}$/$ADP_{13.5}$ remarkably reduces to ~193 kW/m^2, as compared to 290.5 kW/m^2 of PA6/ADP_{18} and 275.4 kW/m^2 of pristine PA6. Such an incredible decline in combustion intensity is associated with the obviously increased char residue from 3.7 wt% of PA6 to 13.5 wt% of PA6/$MPA_{4.5}$/$ADP_{13.5}$. Besides, the average effective heat of combustion (AEHC) of FRPA6 samples presents a distinct decline as compared to that of pure PA6, revealing good flame inhibition in the gas phase. Particularly, for PA6/$MPA_{4.5}$/$ADP_{13.5}$, its EHC reduces from 29.7 MJ/kg of pure PA6 to 24.2 MJ/kg. Obviously, the significant reduction in combustion intensity of FRPA6 composites results from the synergistic effect between MPA and ADP.

The FPI and FGI values are presented in Fig. 4(a) and Table 4. Generally, a high FPI indicates low flashover inclination and a low FGI represents slow fire propagation [48]. Apparently, PA6/MPA_5/ADP_{13} and PA6/$MPA_{4.5}$/$ADP_{13.5}$ exhibit the highest FPI value (0.21 kW/(m^2 s)) and the latter presents the lowest FGI value (0.99 (m^2 s)/kW), indicative of their better fire safety.

Table 3
Cone calorimetry test results of PA6 and FRPA6.

Sample	TTI[a] (s)	PHRR[b] (kW/m^2)	THR[c] (MJ/m^2)	AEHC[d] (MJ/Kg)	MARHE[e] (kW/m^2)	Residue (wt%)	Mean COY[f] (kg/kg)	Mean CO_2Y[f] (kg/kg)
PA6	102	522.1	106.5	29.7	275.4	3.7	0.02	1.87
PA6/MPA_{18}	40	597.7	85.9	26.0	331.1	12.0	0.02	1.64
PA6/MPA_6/ADP_{12}	58	334.2	83.7	24.3	228.7	10.9	0.10	1.39
PA6/MPA_5/ADP_{13}	60	280.9	86.3	25.0	193.1	10.8	0.10	1.40
PA6/$MPA_{4.5}$/$ADP_{13.5}$	58	272.9	78.3	24.2	194.3	13.5	0.10	1.38
PA6/$MPA_{3.6}$/$ADP_{14.4}$	53	297.2	82.1	24.7	193.6	14.3	0.09	1.41
PA6/MPA_3/ADP_{15}	60	313.9	83.7	24.5	206.8	13.3	0.10	1.39
PA6/ADP_{18}	61	442.6	91.2	25.3	290.5	8.2	0.10	1.46

[a] TTI: Time to ignition;
[b] PHRR: Peak heat rate release;
[c] THR: Total heat release;
[d] AEHC: Average effective heat of combustion;
[e] MARHE: Maximum average rate of heat emission;
[f] Mean COY and Mean CO_2Y: mean CO and CO_2 yields.

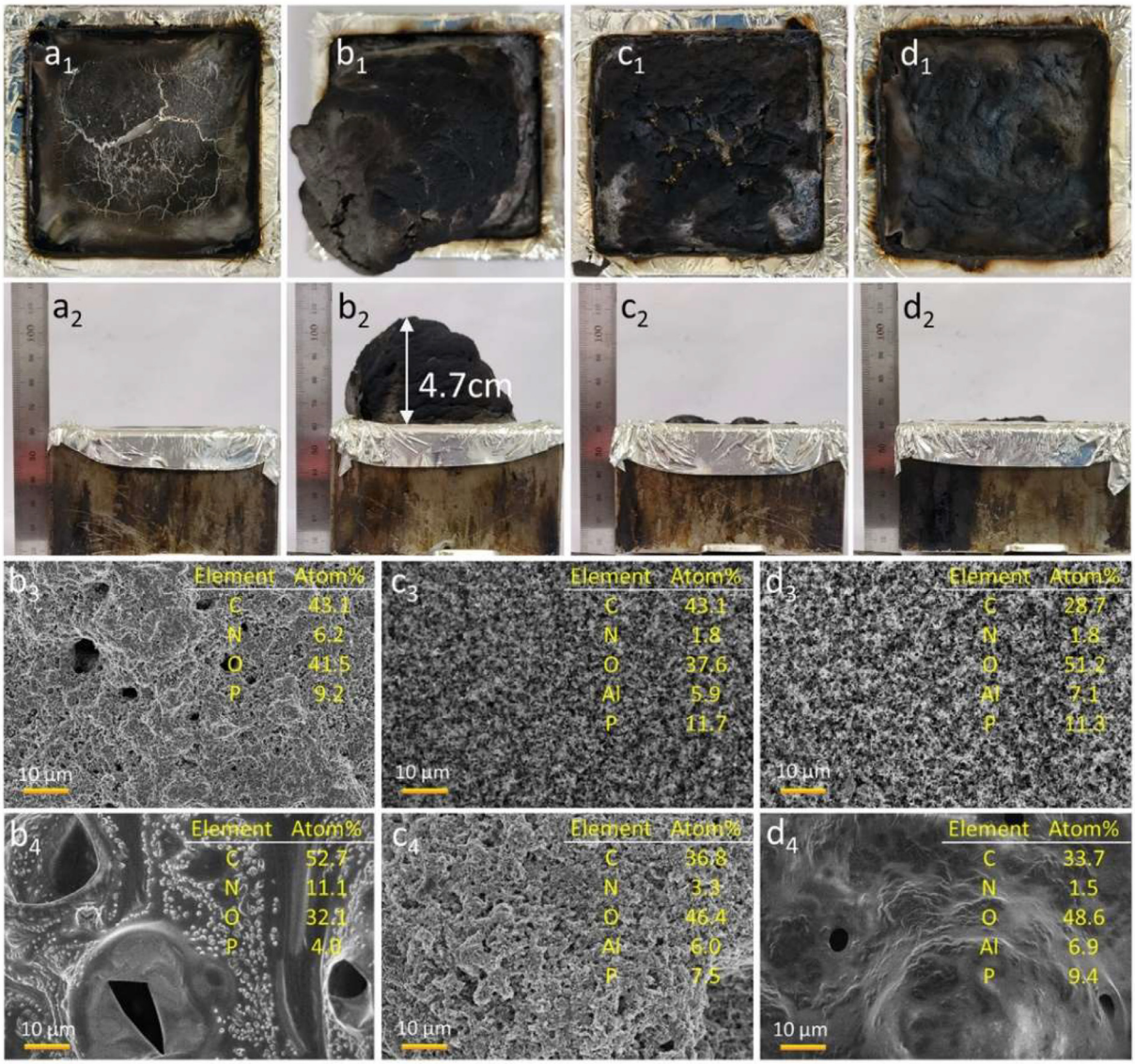

Fig. 5. Digital photos (a_1–d_2) of chars after cone calorimeter tests for (a) PA6, (b) PA6/MPA_{18}, (c) PA6/$MPA_{4.5}$/$ADP_{13.5}$, and (d) PA6/ADP_{18} from top and side views, and SEM images and element compositions obtained from EDS of external (b_3–d_3) and internal (b_4–d_4) chars after cone calorimeter tests for (b) PA6/MPA_{18}, (c) PA6/$MPA_{4.5}$/$ADP_{13.5}$, and (d) PA6/ADP_{18}.

The synergistic effect (SE) in terms of PHRR, THR, and EHC are presented in Fig. 4(b) and Table 4. PA6/$MPA_{4.5}$/$ADP_{13.5}$ achieves the highest synergistic efficiency, such as an SE of 42.9 % for PHRR and an SE of 12.4 % for THR. Though its EHC SE is slightly lower than that of PA6/MPA_6/ADP_{12}, its value remains higher than those of the other three FRPA6 composites. When the appropriate proportion (especially 3:1) of ADP and MPA is added with a total loading level kept at 18 wt%, the outstanding synergistic effects on reducing the flammability of PA6 can be achieved.

3.4. Fire-retardant mechanism

3.4.1. Char residue analysis

To better understand the mechanism of MPA in the condensed phase, the morphologies of FRPA6 char residues recorded by digital photo and SEM are presented in Fig. 5. Pure PA6 produces very few char residues due to its high flammability (see Fig. 5(a_1, a_2). The addition of 18 wt% MPA enables PA6 to generate much swollen char residue as presented in Fig. 5(b_1, b_2). Although the char height reaches ~4.7 cm, there are many cavities in external and internal layers (see Fig. 5(b_3, b_4)), which are conducive to gas and heat exhalation, leading to the increased PHRR and MARHE values. As expected, PA6/$MPA_{4.5}$/$ADP_{13.5}$ generates more compact char residue after combustion as shown in Fig. 5(c_1–c_4), which is responsible for the obviously reduced heat release rate. Similar to PA6/MPA_{18}, there are many holes in the char layer, especially internal layer of PA6/ADP_{18} (Fig. 5(d_1–d_4)). All these results indicate that MPA and ADP synergistically function in the char formation, bringing about superior fire retardancy.

EDS and XPS were also used to study the difference in char quality from the perspective of elemental composition (see Fig. 5, Fig. 6 and Table S2) [49]. For PA6/MPA_{18}, although its char contains a certain amount of N and P in both inner and external char layers, it is difficult to form a dense char barrier due to the mass release of the inert gas (proved by TG-IR). For PA6/$MPA_{4.5}$/$ADP_{13.5}$ and PA6/ADP_{18}, Al element participates in the char-formation, besides C, N, O, and P (see Fig. 6(b_1, c_1)). Although the char of PA6/$MPA_{4.5}$/$ADP_{13.5}$ shows lower (or close) Al and P proportions, it has a higher C/O ratio (0.79) and a lower P/O ratio (0.16) in its inner structure than PA6/ADP_{18} (0.69 and 0.19). This suggests

Table 4
Fire performances and synergistic efficiencies of PA6 and FRPA6.

Sample	FPI[a] (kW/(m^2 s))	FGI[b] ((m^2 s)/kW)	PHRR SE[c] (%)	THR SE (%)	EHC SE (%)
PA6	0.20	1.58	–	–	–
PA6/MPA$_{18}$	0.07	3.23	–	–	–
PA6/MPA$_6$/ADP$_{12}$	0.17	1.34	32.4	6.4	4.6
PA6/MPA$_5$/ADP$_{13}$	0.21	3.12	42.2	3.9	1.8
PA6/MPA$_{4.5}$/ADP$_{13.5}$	0.21	0.99	42.9	12.4	4.4
PA6/MPA$_{3.6}$/ADP$_{14.4}$	0.18	3.72	37.2	9.0	2.8
PA6/MPA$_3$/ADP$_{15}$	0.19	3.14	33.0	7.3	3.6
PA6/ADP$_{18}$	0.14	1.84	–	–	–

[a] FPI: Fire performance index;
[b] FGI: Fire growth index;
[c] SE: Synergistic effect.

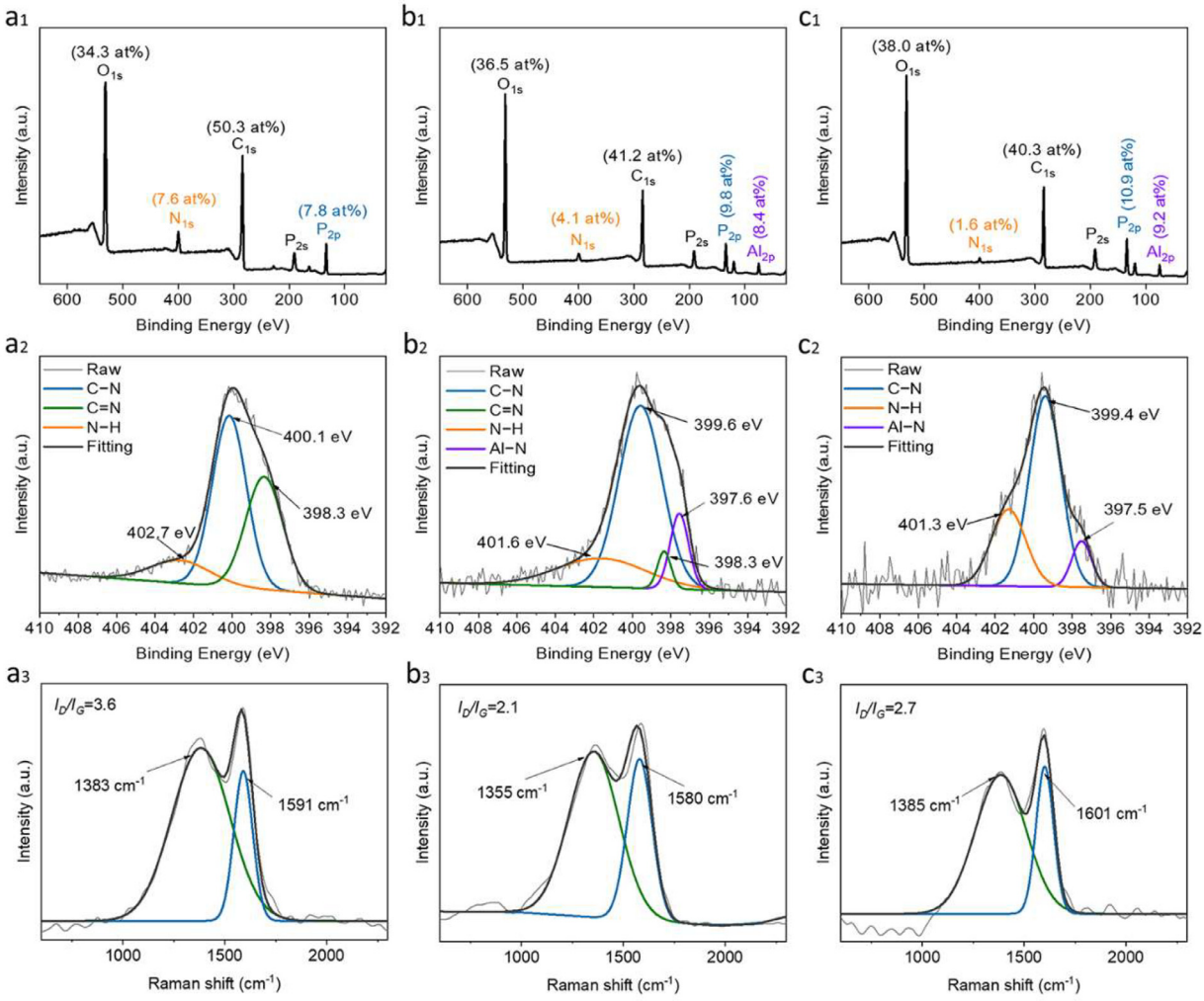

Fig. 6. (a_1–c_1) XPS survey spectra, (a_2–c_2) high resolution N_{1s} XPS spectra and (a_3–c_3) Raman spectra of PA6/MPA$_{18}$, PA6/MPA$_{4.5}$/ADP$_{13.5}$ and PA6/ADP$_{18}$ chars after cone calorimetry tests.

that the char of PA6/MPA$_{4.5}$/ADP$_{13.5}$ has more (poly)phosphate but fewer C–O structures, thus enabling it to achieve higher compactness (see Fig. 5(c_3, c_4)). It is also noted that more N element (4.1 %) gets involved in char-forming for the synergistic formula compared to PA6/ADP$_{18}$ (1.6 %). Apart from the C–N and Al–N bonds, the C=N (from triazine rings) structure exists in the char (see Fig. 6(b_2, c_2)), which also contributes to the generation of a denser char layer [23,50,51]. The high-quality char is also demonstrated by its higher graphitization degree, which can be reflected by the intensity proportion of D peak to G peak (I_D/I_G) in the Raman spectrum. The lower I_D/I_G value indicates a higher graphitization degree [13,52]. As presented in Fig. 6(a_3–c_3), the PA6/MPA$_{4.5}$/ADP$_{13.5}$ char possesses the lowest I_D/I_G value (2.1) than the PA6/MPA$_{18}$ (3.6) and PA6/ADP$_{18}$ (2.7) chars, illustrating that it has the best barrier effect in the condensed phase.

3.4.2. Pyrolysis product analysis

The evolved thermal degradation profiles of FRPA6 composites are demonstrated by TG-IR. For PA6/MPA$_{18}$ (see Fig. 7(a_1, a_2)), it begins to thermally decompose at 350 °C, and then the typical absorption peaks of the degradation production from the PA6 matrix appear when the temperature reaches 400 °C, such as 2980, 2865,

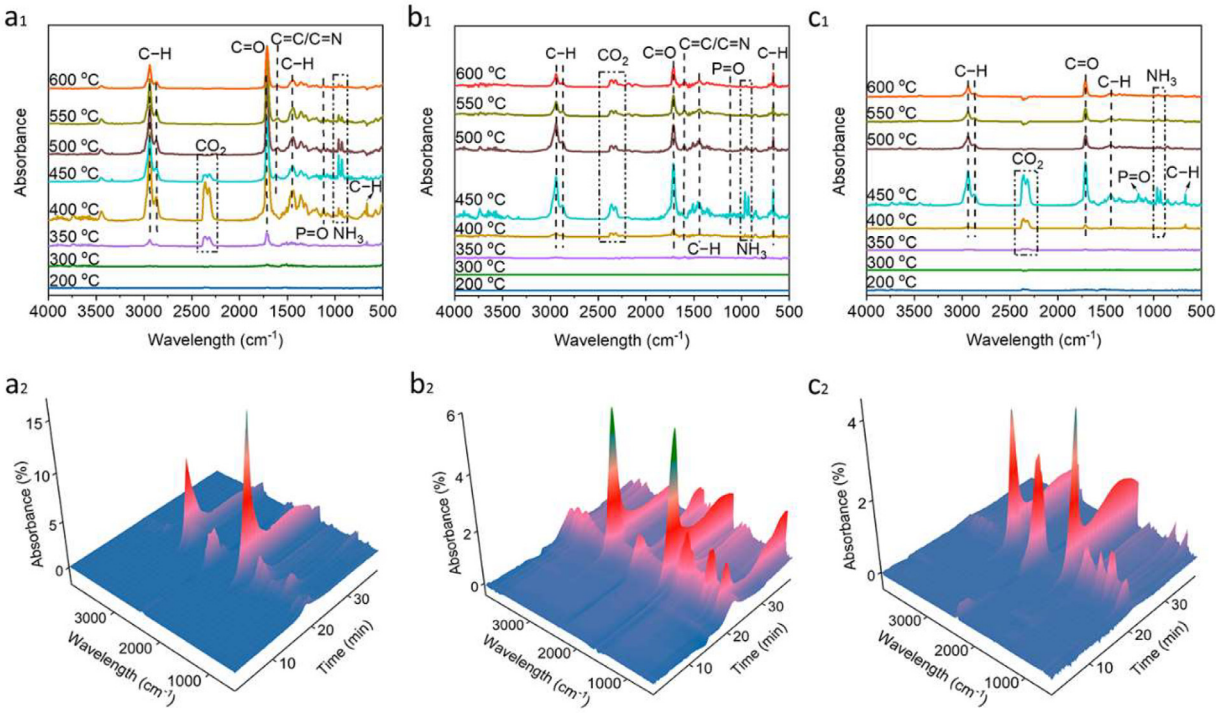

Fig. 7. TG-IR spectra (2D and 3D) of gaseous products of (a_1, a_2) PA6/MPA_{18}, (b_1, b_2) PA6/$MPA_{4.5}$/$ADP_{13.5}$, and (c_1, c_2) PA6/ADP_{18} at different temperatures.

and 1440 cm^{-1} for C–H and 1708 cm^{-1} for C=O [53]. The characteristic absorption peak of NH_3 (967/928 cm^{-1}) also emerges at 400 °C, and then becomes strong at 450°C, indicating the mass release of the decomposition fragments from MPA into the gas phase. This NH_3 peak still exists even at 500 °C and above, which implies that abundant NH_3 is released during the decomposition of PA6/MPA_{18}. However, excessive gas source (ammonia) damages the char layers, reducing the compactness (see Fig. 5(b_1–b_4)) and then leading to higher heat/gas release during combustion. Meanwhile, the weak P=O absorption at 1110 cm^{-1} during the whole thermal decomposition explains the reason why the PA6/MPA_{18} sample is flammable (few radical-trapping effect).

In comparison, PA6/$MPA_{4.5}$/$ADP_{13.5}$ and PA6/ADP_{18} present higher thermal stability. As shown in Fig. 7(b_1–c_2), PA6/$MPA_{4.5}$/$ADP_{13.5}$ and PA6/ADP_{18} do not present distinct decompose products until the temperature reaches 400°C. Moreover, their NH_3 production gradually reduces above 450 °C and the corresponding IR absorption disappears above 500 °C. Such limited inert gas release facilitates the formation of intact and dense char residues (see Fig. 5(c_1–d_4)). Particularly for PA6/ADP_{18}, it shows clear P=O absorption, implying the existence of PO• in the gas phase. Obviously, the mass production of PO• with flame inhibition effect in the gas phase is responsible for the excellent fire resistance of PA6/ADP_{18} (a LOI of 34.1 % and a UL-94 V-0 rating).

3.4.3. Calculational mechanism assessment

The flame inhibition, charring effect, and barrier-protective effect are obtained from cone calorimetry tests (see Fig. 8 and Table S3). Approximately parallel flame inhibition values of FRPA6 composites reveal their similar gas-phase modes of action. PA6/$MPA_{4.5}$/$ADP_{13.5}$ composite presents superior charring effect (9.9 %) and barrier-protective effect (28.9 %), apart from the high flame inhibition (18.5 %). The undesired charring effect (−1.1 %) for PA6/ADP_{18} reveals the moderate charring ability of ADP, which is compatible with the above results. PA6/MPA_{18} shows an extremely low barrier-protection effect (−41.9 %), which is ascribed to the incompact char residue. Accordingly, MPA can exert a certain flame inhibition effect by releasing inert gases (NH_3) and P/O-containing free radicals into the gas phase during combustion, but it suffers from the adverse effect on increasing the char compactness in the condensed phase. Hence, the single use of ADP or MPA cannot simultaneously achieve fire-retardant effect in both condensed and gas phases, and the combination of ADP and MPA contributes to exerting dual-phase fire-retardant effect.

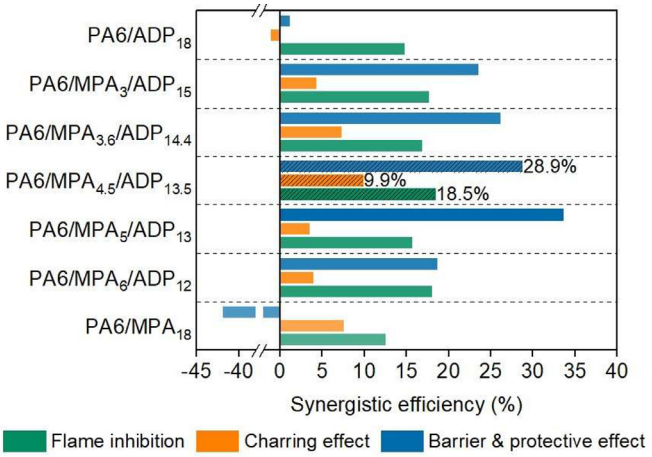

Fig. 8. Fire retardant mechanism of FRPA6 samples in terms of flame inhibition, charring, and barrier-protective layer effects.

3.5. Mechanical performances

The mechanical properties of pristine PA6 and FRPA6 composites are displayed in Fig. S2 and Table S4. Pristine PA6 exhibits high mechanical performances with a tensile strength of ~47.1 MPa, an elastic modulus of ~847 MPa, and an elongation at a break of ~150 %. The addition of fire retardants inevitably reduces the me-

chanical properties of PA6 to some extent. For example, the addition of 18 wt% commercial ADP substantially decreases the tensile strength and elongation at break to 32.8 MPa and 13.6 %, respectively. By comparison, PA6/MPA_{18} presents a higher tensile strength of 37.1 MPa but is more brittle with an elongation at a break of 7.8 %. Expectedly, combining MPA and ADP endows PA6 with moderate tensile strength (such as 36.0 MPa for PA6/$MPA_{4.5}$/$ADP_{13.5}$), but improved ductility. For instance, the elongation at break of PA6/$MPA_{4.5}$/$ADP_{13.5}$ is up to 27.3 % (nearly twice as high as that of PA6/ADP_{18}). Besides, the elastic modulus of all FRPA6 composites significantly rises, e.g., ~1500 MPa for PA6/$MPA_{4.5}$/$ADP_{13.5}$ (almost 80 % higher than that of pure PA6). In summary, the synergistic system (MPA/ADP) allows FRPA6 composites to realize acceptable mechanical strength and superior rigidity.

4. Conclusion

A bio-based MPA is prepared via a facile and environmentally friendly reaction in this study. MPA presents strong fire-retardant synergism with ADP towards PA6. Specifically, the combined addition of 4.5 wt% MPA and 13.5 wt% ADP (weight ratio of MPA/ADP = 1/3) allows PA6 to achieve 47.8 % and 26.5 % reductions in PHRR and THR, respectively, compared to those of pristine PA6. Meanwhile, such formula shows the highest synergistic efficiencies in PHRR (42.9 %) and THR (12.4 %), as well as a high LOI value (29.7 %) and an UL-94 V-0 rating. The excellent fire safety of FRPA6 is ascribed to the exceptional barrier effect of the compact char residue and the flame inhibition effect in the gas phase. This study offers a facile and green approach to designing bio-based flame-retardant synergists for creating high-performance PA6 materials with superior fire safety and desired thermal stability.

Declaration of competing interest

The authors declare that they have no known competing financial interests or personal relationships that could have appeared to influence the work reported in this paper.

Acknowledgments

This work was financially supported by the Australian Research Council (Grant Nos. FT190100188, LP220100278, DP240102628, DP240102728). Thanks are given to both Professor Juan Li of NingboTech University and Professor Miaojun Xu of Northeast Forestry University for their help in fire testing.

Supplementary materials

Supplementary material associated with this article can be found, in the online version, at doi:10.1016/j.jmst.2024.03.001.

References

[1] W. He, H. Xu, P. Song, Y. Xiang, S. Qin, Polym. Degrad. Stabil. 196 (2022) 109847 -0857.
[2] W. Wang, F. Wang, H. Li, Y. Liu, J. Appl. Polym. Sci. 140 (2023) e53536.
[3] Q. Zhang, G.R. Zhu, X.X. Xiao, Q.S. Liu, M. Jiang, D.M. Guo, H.B. Zhao, W.D. Li, L. Chen, B.W. Liu, Y.Z. Wang, Chem. Eng. J. 472 (2023) 144983–144993.
[4] W. He, J. Gao, S. Liao, X. Wang, S. Qin, P. Song, Compos. Commun. 13 (2019) 143–150.
[5] Y. Li, J. Wang, B. Xue, S. Wang, P. Qi, J. Sun, H. Li, X. Gu, S. Zhang, Chemosphere 287 (2022) 132100–132109.
[6] X. Zheng, Y. Li, J. Tang, G. Yu, ACS Omega 7 (2022) 12772–12778.
[7] M.M. Velencoso, A. Battig, J.C. Markwart, B. Schartel, F.R. Wurm, Angew. Chem. Int. Edit. 57 (2018) 10450–10467.
[8] K. Salasinska, K. Mizera, M. Celiński, P. Kozikowski, M. Borucka, A. Gajek, Fire Saf. J. 115 (2020) 103137–103151.
[9] S. Huo, P. Song, B. Yu, S. Ran, V.S. Chevali, L. Liu, Z. Fang, H. Wang, Prog. Polym. Sci. 114 (2021) 101366–101401.
[10] Y. Wang, J. Deng, J. Zhao, H. Shi, Prog. Org. Coat. 158 (2021) 106346–106356.
[11] J. Feng, Y. Lu, H. Xie, Z. Xu, G. Huang, C.F. Cao, Y. Zhang, V.S. Chevali, P. Song, H. Wang, ACS Sustain. Chem. Eng. 10 (2022) 15223–15232.
[12] J. Feng, Z. Ma, Z. Xu, H. Xie, Y. Lu, C. Maluk, P. Song, S. Bourbigot, H. Wang, Chem. Eng. J. 431 (2022) 134259–134271.
[13] J. Feng, Y. Lu, H. Xie, Y. Zhang, S. Huo, X. Liu, M. Flynn, Z. Xu, P. Burey, M. Lynch, H. Wang, P. Song, J. Mater Sci. Technol. 160 (2023) 86–95.
[14] X. Zhong, X. Yang, K. Ruan, J. Zhang, H. Zhang, J. Gu, Macromol. Rapid Commun. 43 (2022) 2100580–2100588.
[15] Y. Liu, A. Zhang, Y. Cheng, M. Li, Y. Cui, Z. Li, Polym. Test. 124 (2023) 108100–108116.
[16] C. Zuo, Y. Guo, L. Jiang, D. Yu, X. Chen, Y. Ren, X. Liu, Eur. Polym. J. 196 (2023) 112304–112316.
[17] Y. Yu, C. Ma, H. Zhang, Y. Zhang, Z. Fang, R. Song, Z. Lin, J. Feng, P. Song, Mater. Today Chem. 30 (2023) 101565–101574.
[18] Y. Xue, T. Zhang, H. Peng, Z. Ma, M. Zhang, M. Lynch, T. Dinh, Z. Zhou, Y. Zhou, P. Song, Nano Res. 17 (2024) 2186 –2184.
[19] F. Safdar, M. Ashraf, A. Abid, A. Javid, K. Iqbal, Mater. Chem. Phys. 311 (2024) 128568–128579.
[20] D. Wang, Y. Wang, X. Zhang, T. Li, M. Du, M. Chen, W. Dong, New J. Chem. 45 (2021) 13329–13339.
[21] W.J. Jin, W.L. He, L. Gu, X.W. Cheng, J.P. Guan, Eur. Polym. J. 180 (2022) 111610 –111610.
[22] K. Sykam, M. Försth, G. Sas, Á. Restás, O. Das, Ind. Crop. Prod. 164 (2021) 113349–113364.
[23] S. Li, F. Zhao, X. Wang, Z. Liu, J. Guo, Y. Li, S. Tan, Z. Xin, S. Zhao, L. Li, Polym. Degrad. Stabil. 219 (2024) 110597–110608.
[24] W. Liu, R. Shi, X. Ge, H. Huang, X. Chen, M. Mu, Prog. Org. Coat. 156 (2021) 106271–106281.
[25] J. Zhong, E. Wang, Y. Sun, N. Yin, S. Tian, W. Ying, W. Li, W. Zhang, Polymers (Basel) 15 (2023) 360–375.
[26] R.K. Jian, X.B. Lin, Z.Q. Liu, W. Zhang, J. Zhang, L. Zhang, Z. Li, D.Y. Wang, Compos. Pt. B-Eng. 200 (2020) 108349–108358.
[27] W.G. Gong, M. Fan, J. Luo, J. Liang, X. Meng, Polym. Adv. Technol. 32 (2021) 1548–1559.
[28] Y. Xu, J. Li, R. Shen, Z. Wang, P. Hu, Q. Wang, J. Therm. Anal. Calorim. 146 (2021) 153–164.
[29] Z. Liu, S. Shang, K. l. Chiu, S. Jiang, F. Dai, Polym. Degrad. Stabil. 167 (2019) 277–282.
[30] S. Shang, B. Yuan, Y. Sun, G. Chen, C. Huang, B. Yu, S. He, H. Dai, X. Chen, J. Colloid Interface Sci. 553 (2019) 364–371.
[31] L. Adlnasab, M. Ezoddin, R.A. Shojaei, F. Aryanasab, J. Chromatogr. B 1095 (2018) 226–234.
[32] Q. Zhang, J. Wang, S. Yang, J. Cheng, G. Ding, S. Huo, Compos. Pt. B-Eng. 177 (2019) 107380–107389.
[33] S. Huo, Z. Liu, J. Wang, J. Therm. Anal. Calorim. 139 (2020) 1099–1110.
[34] M. Čolović, J. Vasiljević, Ž. Štirn, N. Čelan Korošin, M. Šobak, B. Simončič, A. Demšar, G. Malucelli, I. Jerman, Chem. Eng. J. 426 (2021) 130760–130774.
[35] M. Xu, X. Li, B. Li, Fire Mater. 40 (2016) 848–860.
[36] Z. Zheng, S. Liu, B. Wang, Y. Ting, X. Cui, H. Wang, Polym. Compos. 36 (2015) 1606–1619.
[37] Y. Gao, C. Deng, Y. Du, S. Huang, Y. Wang, Polym. Degrad. Stabil. 161 (2019) 298–308.
[38] X. Cheng, Y. Wu, B. Hu, J. Guan, Surf. Innov. 8 (2020) 315–322.
[39] Y. Wang, D. Wang, M. Zhang, D. Wang, T. Li, J. Jiang, M. Chen, W. Dong, Polym. Degrad. Stabil. 211 (2023) 110309–110318.
[40] W. Tao, J. Li, Appl. Surf. Sci. 456 (2018) 751–762.
[41] U. Braun, H. Bahr, B. Schartel, e-Polymers 10 (2010) 041.
[42] H. Feng, Y. Qiu, L. Qian, Y. Chen, B. Xu, F. Xin, Polymers (Basel) 11 (2019) 1–13.
[43] T. Liang, J. Cai, S. Liu, H. Lai, J. Zhao, Materials (Basel) 12 (2019) 2217–2233.
[44] Y. Lu, J. Feng, D. Yi, H. Xie, Z. Xu, C.F. Cao, S. Huo, H. Wang, P. Song, Compos. Pt. A-Appl. Sci. Manuf. 176 (2024) 107834–107843.
[45] W.X. Li, H.J. Zhang, X.P. Hu, W.X. Yang, Z. Cheng, C.Q. Xie, J. Hazard. Mater. 398 (2020) 123001–123013.
[46] J. Zhang, Y. Fang, A. Zhang, Y. Yu, L. Liu, S. Huo, X. Zeng, H. Peng, P. Song, Prog. Org. Coat. 185 (2023) 107910–108919.
[47] Z. Li, Q. Liu, S. Tang, D. Feng, W. Zhao, B. Li, D. Xie, Y. Mei, Colloid Surf, A Physicochem. Eng. Asp. 664 (2023) 131198–131212.
[48] B. Yu, B. Tawiah, L.Q. Wang, A.C.Y. Yuen, Z.C. Zhang, L.L. Shen, B. Lin, B. Fei, W. Yang, A. Li, S.E. Zhu, E.Z. Hu, H.D. Lu, G.H. Yeoh, J. Hazard. Mater. 374 (2019) 110–119.
[49] L. Tang, K. Ruan, X. Liu, Y. Tang, Y. Zhang, J. Gu, Nano-Micro Lett. 16 (2024) 38.
[50] C.F. Cao, B. Yu, Z.Y. Chen, Y.X. Qu, Y.T. Li, Y.Q. Shi, Z.W. Ma, F.N. Sun, Q.H. Pan, L.C. Tang, P. Song, H. Wang, Nano-Micro Lett. 14 (2022) 92–109.
[51] Q. Liu, D. Feng, W. Zhao, D. Xie, Y. Mei, Polym. Degrad. Stabil. 206 (2022) 110201–110213.
[52] L. Wang, X. Shi, J. Zhang, Y. Zhang, J. Gu, J. Mater Sci. Technol. 52 (2020) 119–126.
[53] S. Hao, D. Feng, F. Wu, Y. Xie, Z. Xu, W. Zhao, D. Xie, Polym. Degrad. Stabil. 218 (2023) 110548–110561.